AIAA JOURNAL
Vol. 47, No. 2, February 2009

Technical Notes

TECHNICAL NOTES are short manuscripts describing new developments or important results of a preliminary nature. These Notes should not exceed 2500 words (where a figure or table counts as 200 words). Following informal review by the Editors, they may be published within a few months of the date of receipt. Style requirements are the same as for regular contributions (see inside back cover).

Flat-Plate Interaction with the Near Wake of a Square Cylinder

Con J. Doolan*
University of Adelaide,
Adelaide, South Australia 5005, Australia

DOI: 10.2514/1.40503

I. Introduction

BLUFF bodies are integral components of aircraft, high-speed trains, automobiles, and many forms of industrial equipment. The minimization of mean and fluctuating force levels generated by bluff bodies when placed in a fluid stream has the benefits of reducing drag, vibration, and radiated sound. It is therefore very important that a good understanding of the flowfield about bluff bodies be obtained to achieve these aims. This Note explores how low Reynolds number bluff-body wake interference can affect the generation of unsteady flow and force. The case chosen for study is the interaction of a square cylinder and an infinitely thin flat plate.

A rigid square cylinder is one of the most basic forms of a bluff body and when placed in a uniform fluid stream has been shown to exhibit strong vortex shedding, resulting in fluctuating forces and the radiation of sound in the form of an aeolian tone. Previous fluid dynamic experimental studies [1,2] exhibit this strong vortex shedding over a wide range of Reynolds number (10^2–10^6). Numerical studies investigating the fluid dynamics [3–6] also confirm this behavior.

Despite the wealth of experimental data available for circular cylinders, experimental or numerical data for square cylinders are rare. Available studies include the work of Inoue [7], who performs a numerical simulation of compressible flow about a square cylinder at $Re = 150$. Zhou et al. [8] use an upstream plate to suppress fluctuating lift on a square cylinder. They find that there is an optimal position and size for the upstream plate for effective lift suppression. Studies concerning the control of noise from a circular cylinder are more common. Recent numerical studies [9,10] investigate the use of a splitter plate attached to the base of a circular cylinder. These studies show that vortex shedding can disappear once the splitter plate achieves a certain length.

Numerical solutions of the compressible unsteady Navier–Stokes equations for tandem square cylinders [11] show that significant force and noise reduction can occur if the cylinders are placed at a critical spacing in a region in which vortex shedding from the upstream cylinder is suppressed. If this separation distance is increased, the force and noise increase rapidly, due to the reestablishment of upstream vortex shedding and the associated vortex impingement on the downstream cylinder.

Other work includes the experimental time-resolved force measurements of tandem bluff bodies by Sakamoto et al. [12] and Alam and Zhou [13], which were used to investigate the phase difference between the aerodynamic forces of each body in the vortex-shedding regime (i.e., the interbody spacing was such that vortex shedding was allowed to occur from each body). In each case, the phase varied linearly with separation distance. Further, Alam and Zhou developed a theoretical model based on the convective properties of isolated bluff-body wakes that agrees reasonably with experimental results.

This Note will consider the case of an infinitely thin flat plate placed in the near wake of a square cylinder at a Reynolds number of $Re = 150$. To the author's knowledge, there have been no previous investigations of the interaction of a thin flat plate with the near wake of a square cylinder. The Note is structured as follows. After outlining the numerical approach (Sec. II), a solution of the incompressible Navier–Stokes equations for the single square cylinder case is presented and validated against available experimental and numerical results (Sec. III). A second solution is then presented that includes the downstream plate (Sec. IV), and the flow and force results are analyzed. The Note concludes with a summary of the key results.

II. Numerical Approach

A. Methodology

The two-dimensional incompressible Navier–Stokes equations were solved using the finite volume OpenFOAM [14] numerical simulation system. The pressure-implicit split-operator algorithm with two correction steps was used as an implicit transient-solution scheme. The resulting system of equations was solved using the incomplete Choleski conjugate gradient method with a solution tolerance of 10^{-6}. Convection terms were discretised using a second-order-accurate technique, and viscous derivatives were approximated using second-order central differencing.

A two-dimensional formulation was chosen for this work, as experimental [15,16] and numerical [5] studies show that the onset of spanwise instabilities occurs above a Reynolds number ($Re = UD/\nu$) of 160 for single square cylinders. All simulations were performed at $Re = 150$, making a two-dimensional study appropriate. It is not known if three-dimensional effects are important for the case in which the square cylinder interacts with a flat plate at $Re = 150$, as this is the first investigation of this system. Given its similarity with the single square cylinder case, a two-dimensional assumption appears to be appropriate.

B. Computational Details

Two computational domains were constructed for this study. The first consisted of a single square cylinder of side length $D = 1$ and extended a distance of 10 cylinder diameters upstream and 20 cylinder diameters in the downstream and cross-stream directions. The second domain consisted of a square cylinder of side length $D = 1$ and an infinitely thin flat plate of chord $C/D = 0.834$ placed $L/D = 2.37$ behind the square cylinder. This second domain also extended a distance of 10 cylinder diameters upstream and 20 cylinder diameters in the downstream (from the plate trailing edge) and cross-stream directions.

Received 19 August 2008; revision received 16 November 2008; accepted for publication 18 November 2008.

*Senior Lecturer, School of Mechanical Engineering; con.doolan@adelaide.edu.au. Senior Member AIAA.

In each domain, a conventional inlet boundary condition was applied to the upstream boundary. Outlet boundary conditions were applied on the remaining external boundaries. A zero-velocity boundary condition was applied to the fixed surfaces of the cylinder and plate.

Simulations were performed using a number of grid resolutions and time steps ($\Delta tU_\infty/D$), and a subset of results are shown in Table 1. All time steps were chosen so that the maximum Courant–Friedrichs–Lewy (CFL) number was below 0.5. The exception is case 4, in which a maximum CFL number of 0.25 was maintained. The results show that the solutions are well converged, with relatively minor variations in fundamental Strouhal number St, cylinder mean drag $\bar{C}_{D_C}$, and cylinder root-mean-square lift coefficient $C_{L'_C}$. For the rest of the Note, results are presented from cases 3 and 7. In each case, the grid is compressed toward the cylinder wall, and for cases 3 and 7, the grid height at the surface was set to $\Delta/D = 0.0167$.

In all cases, the solution was commenced with uniform initial velocity across the flow domain and at the inlet (i.e., $U_1/U_\infty = 1$), and vortex shedding initiated itself naturally. Statistically stationary flow was established at a nondimensional time of $tU_\infty/D = 150$. Flow sampling occurred over a nondimensional time of $tU_\infty/D = 250$, which equates to approximately 37 vortex-shedding cycles. Additional simulations were performed for case 7 over a time range $400 \leq tU_\infty/D \leq 407$ for flow visualization purposes.

III. Evaluation of Single-Cylinder Numerical Data

A. Flow Visualization

Figure 1 shows contours of instantaneous nondimensional vorticity magnitude ($|\Omega|D/U_\infty$, where $|\Omega| = \sqrt{\Omega_i^2}$ is the vorticity magnitude) around the single cylinder (case 3) at a nondimensional time of $tU_\infty/D = 400$. Strong vortex shedding is observed, in line with previous experimental [2] and numerical [5,11] results. Boundary layers form on the cylinder front surface. They grow from the stagnation zone at the centerline, then separate at the sharp leading-edge corners of the cylinder. The free-shear layers then pass over the entire cylinder without reattaching on its surface. The shear layers then interact with each other in the near wake, forming a von Kármán vortex street behind the cylinder.

B. Fluctuating Aerodynamic Loads

Table 2 compares the numerically computed values of vortex-shedding Strouhal number St, mean drag $\bar{C}_{D_C}$, and root-mean-square lift coefficient $C_{L'_C}$ with those of other studies. Two numerical studies are used for comparison. The first is the incompressible study of Sohankar et al. [5] in which two- and three-dimensional flow over a square cylinder was studied for a range of Reynolds numbers. They found that at $Re = 150$, the two- and three-dimensional flow results were nearly identical; therefore, the two-dimensional results are used for comparison here. The two-dimensional compressible study of flow over a square cylinder at $Re = 150$ by Inoue et al. [11] is also used for validation.

Experimental results from Okajima [2] are used for validation, along with the experimental results listed by Sohankar et al. [5]. There are no available lift data measurements for flow at this Reynolds number.

Fig. 1 Visualization of the instantaneous vorticity magnitude about the single square cylinder (case 3) at $Re = 150$ and $tU_\infty/D = 400$ with 20 equally spaced contours of instantaneous vorticity magnitude over the range $0.2 \leq |\Omega|D/U_\infty \leq 4$.

Table 1 Grid convergence results

Case	Description	Grid	$\Delta tU_\infty/D$	St	$\bar{C}_{D_C}$	$C_{L'_C}$
1	Single cylinder	175×125	0.01	0.156	1.45	0.311
2	Single cylinder	209×150	0.005	0.155	1.44	0.300
3	Single cylinder	250×180	0.005	0.156	1.44	0.296
4	Single cylinder	250×180	0.0025	0.156	1.44	0.293
5	Cylinder plate	255×125	0.01	0.125	1.32	0.065
6	Cylinder plate	301×151	0.005	0.127	1.32	0.062
7	Cylinder plate	360×180	0.005	0.128	1.31	0.062

Table 2 Comparison of numerical frequency and fluctuating force data with experimental and other numerical results

Parameter	Case 3	Sohankar et al. [5]	Inoue et al. [11]	Experiment [2,5]
St	0.156	0.165	0.151	0.148-0.155
$\bar{C}_{D_C}$	1.44	1.44	1.4	1.4
$C_{L'_C}$	0.296	0.23	0.4	——

Inspection of the values of Strouhal numbers in Table 2 shows that the current simulation is in excellent agreement with experimental measurements and is between the values predicted by previous numerical studies. The mean drag coefficient is in excellent agreement with all previous experiments and numerical investigations. Root-mean-square lift coefficient is between the values predicted by previous numerical studies.

IV. Evaluation of Cylinder-plate Numerical Data

A. Flow Visualization

The inclusion of the plate in the near-wake region strongly perturbs the flowfield in a fundamental manner. Strong vortex shedding still occurs, but a complicated flow pattern exists between the cylinder and plate. A detailed inspection of the near-wake flowfield is made in Fig. 2 (case 7), in which the spanwise vorticity is visualized over a complete vortex-shedding cycle. Nine images are shown (with Figs. 2a and 2i being identical), each separated by one nondimensional unit of time. The first image shows positive vorticity over the upper surface of the plate, generated by the proximity of the upper shear layer from the upper leading edge of the square cylinder. The vorticity on the upper surface of the plate has shed forward of the plate leading edge and is beginning to interact with the lower-cylinder shear layer. Negative vorticity is generated at the plate trailing edge, due to the proximity of the nearly fully developed von Kármán vortex that originated from the lower-cylinder shear layer.

In the next image (Fig. 2b), both of the vortical structures developed at the leading and trailing edges of the plate have shed into the surrounding fluid, both in a negative x direction (against the freestream fluid velocity direction). The leading-edge vortex is being dissipated and merged with the lower-cylinder shear layer. The trailing-edge vortex appears to form a jet by combining with the opposite signed lower-shear-layer vorticity and instigates negative vorticity about the front of the lower-plate leading edge.

In the next three images (Figs. 2c–2e), the leading-edge vorticity grows as the lower-cylinder shear layer starts to approach the plate. Similarly, the intensity of the vorticity about the trailing edge grows as the von Kármán vortex forms in the upper-cylinder shear layer. The leading- and trailing-edge plate vorticial structures then shed into the surrounding fluid and the process repeats itself, as shown in the remaining images (Figs. 2f–2i).

A time-varying stagnation zone is also seen to form on the back surface of the cylinder. It is caused by the interaction of the plate with the near-wake flowfield. It can be identified by the vorticity lines joining the surface of the cylinder. The stagnation zone starts near the bottom of the back surface, as shown in Fig. 2a. As the vortex-shedding cycle progresses, the stagnation zone moves to the top of the cylinder back surface and then back down again.

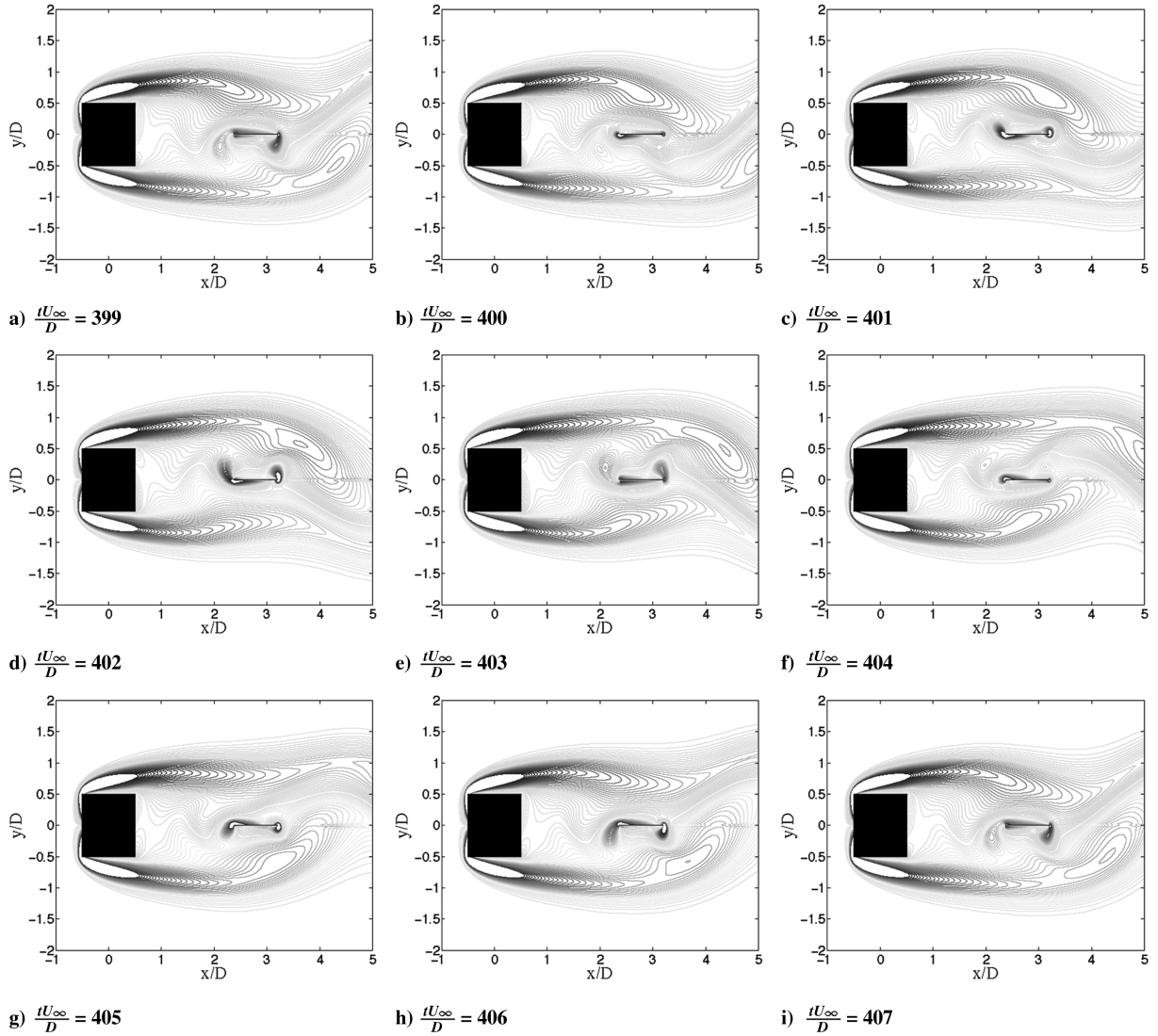

Fig. 2 Visualization of the instantaneous spanwise vorticity field about the square cylinder and plate at $L/D = 2.37$ with $Re = 150$ over a complete vortex-shedding cycle (case 7). Each plot uses 20 equally spaced contours of instantaneous spanwise vorticity over the range $-4 \leq \Omega_z D/U_\infty \leq 4$.

B. Fluctuating Aerodynamic Loads

The power spectral densities of the cylinder and plate lift coefficients are shown in Fig. 3. The addition of the plate results in another tonal component in the force spectra, approximately three times that of the primary vortex-shedding Strouhal number.

Table 3 compares the numerical results from cases 3 and 7. The subscript C refers to the cylinder and the subscript P refers to the plate. The Strouhal number associated with the second peak in the force power spectral densities is labeled St_1. The main shedding frequency has been reduced by the addition of the second plate, as has

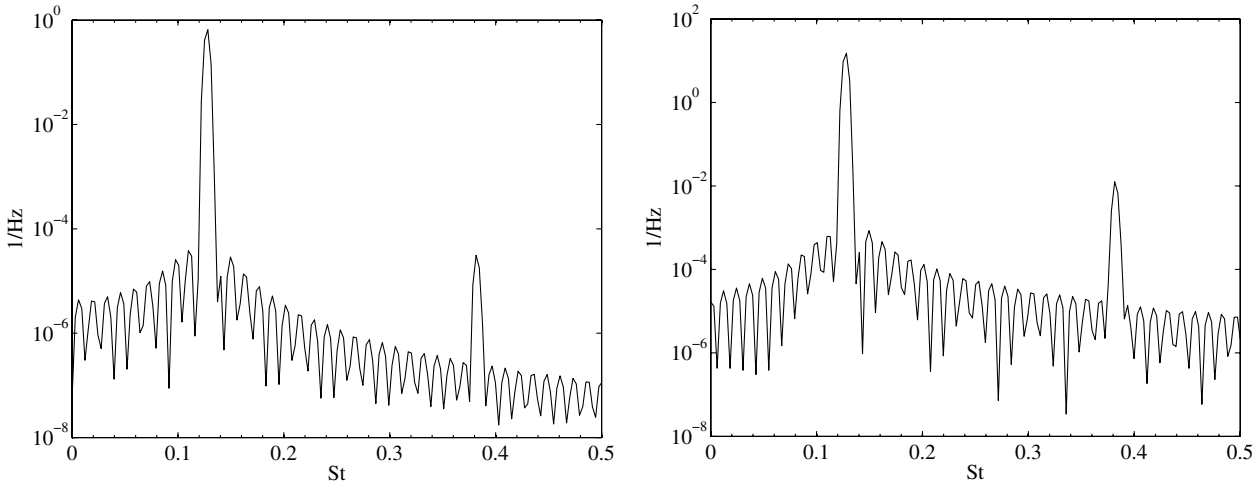

a) Square cylinder **b) Plate**

Fig. 3 Power spectral densities of the cylinder and plate lift coefficients.

Table 3 Comparison of flow parameters for the single-cylinder and cylinder-plate interaction simulations

Parameter	Single cylinder (case 3)	Cylinder plate (case 7)
St	0.156	0.128
St_1	——	0.382
$\bar{C}_{D_C}$	1.44	1.31
$\bar{C}_{D_P}$	——	−0.053
$C_{L'_C}$	0.296	0.062
$C_{L'_P}$	——	0.296

the mean drag coefficient. The root mean square of the cylinder lift coefficient has been dramatically reduced, but the lift coefficient on the plate is the same magnitude of the single-cylinder case.

The mean drag coefficient of the cylinder has also been reduced by the addition of a plate in the near wake. Interestingly, the plate experiences a mean thrust, due to the mean flow near its surface being in the negative streamwise direction.

V. Conclusions

Numerical results for a single square cylinder compare well with available experimental and numerical data at $Re = 150$. The addition of an infinitely thin plate in the near wake resulted in fundamental changes to the flowfield. Key features of the flow between the cylinder and plate are strong secondary vortices at the leading and trailing edges of the plate and a reversed flow environment over the plate.

The wake interference caused by the plate reduced the fundamental Strouhal number and added a second harmonic lift component that oscillated at three times the fundamental Strouhal number. The force on the square cylinder was reduced significantly; however, the amplitude of the lift coefficient on the downstream plate was found to be the same as for the single square cylinder.

Acknowledgments

The author would like to thank Lars Davidson and Chalmers University of Technology for hosting a visit at which this work was performed. This visit was partly funded by the Australian Government Department of Innovation, Industry, Science and Research's International Science Linkages (ISL) program.

References

[1] Norberg, C., "Flow Around Rectangular Cylinders—Pressure Forces and Wake Frequencies," *Journal of Wind Engineering and Industrial Aerodynamics*, Vol. 49, No. 1–3, Jan. 1993, pp. 187–196. doi:10.1016/0167-6105(93)90014-F

[2] Okajima, A., "Strouhal Numbers of Rectangular Cylinders," *Journal of Fluid Mechanics*, Vol. 123, 1982, p. 379. doi:10.1017/S0022112082003115

[3] Davis, R. W., and Moore, E. F., "A Numerical Study of Vortex Shedding from Rectangles," *Journal of Fluid Mechanics*, Vol. 116, Mar. 1982, pp. 475–506. doi:10.1017/S0022112082000561

[4] Kelkar, K. M. and Patankar, S. V., "Numerical Prediction of Vortex Shedding Behind a Square Cylinder," *International Journal for Numerical Methods in Fluids*, Vol. 14, Feb. 1992, pp. 327–341. doi:10.1002/fld.1650140306

[5] Sohankar, A., Norberg, C., and Davidson, L., "Simulation of Three-Dimensional Flow Around a Square Cylinder at Moderate Reynolds Numbers," *Physics of Fluids*, Vol. 11, No. 2, Jan. 1999, pp. 288–306. doi:10.1063/1.869879

[6] Taylor, I., and Vezza, M., "Prediction of Unsteady Flow Around Square and Rectangular Section Cylinders Using a Discrete Vortex Method," *Journal of Wind Engineering and Industrial Aerodynamics*, Vol. 82, Jan. 1999, pp. 247–269. doi:10.1016/S0167-6105(99)00038-0

[7] Inoue, O., "Direct Numerical Simulation of Aeolian Tones," *The 5th Asian Computational Fluid Dynamics Conference*, June 2003, p. 6.

[8] Zhou, L., Cheng, M., and Hung, K., "Suppression of Fluid Force on a Square Cylinder by Flow Control," *Journal of Fluids and Structures*, Vol. 21, No. 2, Nov. 2005, pp. 151–167. doi:10.1016/j.jfluidstructs.2005.07.002

[9] You, D., Choi, H., Choi, M., and Kang, S., "Control of Flow-Induced Noise Behind a Circular Cylinder Using Splitter Plates," *AIAA Journal*, Vol. 36, No. 11, Jan. 1998, pp. 1961–1967. doi:10.2514/2.322

[10] Kwon, K., and Choi, H., "Control of Laminar Vortex Shedding Behind a Circular Cylinder Using Splitter Plates," *Physics of Fluids*, Vol. 8, No. 2, Jan. 1996, pp. 479–486. doi:10.1063/1.868801

[11] Inoue, O., Mori, M., and Hatakeyama, N., "Aeolian Tones Radiated from Flow Past Two Square Cylinders in Tandem," *Physics of Fluids*, Vol. 18, No. 4, Jan. 2006, Paper 046101. doi:10.1063/1.2187446

[12] Sakamoto, H., Haniu, H., and Obata, Y., "Fluctuating Fluid Forces Acting on Two Square Prisms in a Tandem Arrangement," *Journal of Wind Engineering and Industrial Aerodynamics*, Vol. 26, No. 1, Jan. 1987, pp. 85–103. doi:10.1016/0167-6105(87)90037-7

[13] Alam, M. M., and Zhou, Y., "Phase Lag Between Vortex Shedding from Two Tandem Bluff Bodies," *Journal of Fluids and Structures*, Vol. 23, No. 2, Feb. 2007, pp. 339–347. doi:10.1016/j.jfluidstructs.2006.11.003

[14] Weller, H., Tabor, G., Jasak, H., and Fureby, C., "A Tensorial Approach to CFD using Object Orientated Techniques," *Computers in Physics*, Vol. 12, No. 6, 1998, pp. 620–631. doi:10.1063/1.168744

[15] Luo, S., Chew, Y., and Ng, Y., "Characteristics of Square Cylinder Wake Transition Flows," *Physics of Fluids*, Vol. 15, No. 9, 2003, pp. 2549–2559. doi:10.1063/1.1540111

[16] Robichaux, J., Balachandar, S., and Vanka, S., "Three-Dimensional Floquet Instability of the Wake of Square Cylinders," *Physics of Fluids*, Vol. 11, 1999, p. 560. doi:10.1063/1.869930

K. Anderson
Associate Editor